UMERC+METS
2024 Conference

7-9 August | Duluth, MN, USA

Simulation of a Dual-Rotor Ocean Current Turbine with Variable Buoyancy and Lifting Surfaces for Motion Control

Hassan Mokari[a], James VanZwieten[b], Yufei Tang[a], John Sninsky[c]

[a]*Florida Atlantic University, Department of Electrical Engineering and Computer Science, 777 Glades Road, Boca Raton, FL 33431, USA*
[b]*Florida Atlantic University, Department of Ocean and Mechanical Engineering, 101 North Beach Road, Dania Beach, FL 33441, USA*
[c]*Current Kinetics, LLC, 10823 SW 27th Ave., Gainsville, Florida, USA*

Abstract

Open ocean currents provide energy dense resources along the western boundaries of the word's ocean basins. These resources contain average energy densities that can exceed 3 kW/m^2 in select areas with total extractable energy levels of several GW. Nearly all areas where ocean currents exceed 0.5 kW/m^2 in energy density are located within the top 100 m of the water column, where the total water depth exceeds 250 m. For this reason, moored ocean current turbine (OCT) solutions are being pursued to enable the extraction of this resource with variable buoyancy, lifting surfaces, or a combination of the two being considered from altitude control. Dual-rotor designs enable net torque cancelation through counter-rotation, minimizing roll motions and misalignment with the current. In this paper, the numerical modeling and simulation-based performance evaluation for a dual-rotor OCT design that uses coupled variable-buoyancy and lifting surface control (i.e., dual-control) is presented. A rigid body approach is utilized where the OCT is modeled as having 8-degrees of freedom (6 for the main body plus the relative rotation speed of each rotor), in addition to the 3-degrees of freedom assigned to each node within the finite-element, lumped-mass cable model.

Keywords: Renewable Energy, Ocean Current Turbines, Numerical Simulation, Marine Hydrokinetic

1. Introduction

Renewable energy resources, including wind, solar, tidal, wave, and ocean currents, are increasingly being targeted for electricity generation. Ocean current energy has garnered considerable interest due to its substantial energy potential and consistent electricity generation capabilities [1]. However, harnessing electrical energy from open-ocean currents remains in its nascent stages of development [2], necessitating resolution of several technical challenges to enable significant electricity production from this source. The world's major ocean currents include: (i) Atlantic currents: the Gulf Stream, Labrador, and Brazil; (ii) Pacific currents: the California, Kuroshio, and Humboldt; and (iii) Indian Ocean currents: the Indian Monsoon and Agulhas. Among these, only the western boundary currents of the ocean basins possess energy densities suitable for ocean current energy production. The theoretically extractable energy from the Gulf Stream current is estimated at 44 GW [3], with 5 GW attributable to the Florida Current [4], according to a model that considers the cumulative impact of ocean energy harvesting on simplified ocean circulation.

These ocean currents possess substantial amounts of extractable energy and exhibit a high energy density. The kinetic energy density is highly dependent on water depth, with higher energy densities nearly always occurring near the ocean surface [5]. Therefore, ocean current turbines should typically be located near the surface but would benefit from the capability to vary their depth. This allows them to avoid surface waves during storms and to maximize energy production when the most energy-dense currents occur at greater depths. This paper focuses on numerically modeling a dual-rotor ocean current turbine (OCT) with a combined variable-buoyancy and lifting surface control.

2. Ocean Current Turbine Modeling

The presented numerical simulation builds on the algorithms presented in [6], [7]. These new techniques specifically relate to coordinate systems, equations of motion, and actuator models. This section presents the complete model of the dual-rotor dual-control OCT, covering coordinate systems, equations of motion, the blade element momentum rotor model, other hydrodynamic forces, environmental models, and actuator models.

2.1. Overview of the Simulated OCT

This section outlines the OCT system design simulated in this paper. The system builds upon the lifting surface-controlled OCT design proposed in [6], adapting the lifting surfaces to operate in the Gulf Stream off the East Coast of Florida such that they can be rigidly fixed to other components without the need for direct actuation. Instead, a buoyancy tank, with two separated chambers, is used to both change the total mass of the system (including entrained water), as well as very the pitch of the entire turbine to alter the lift forces on the main wing. This design is illustrated in Fig 1, with some components not drawn to scale. The new OCT design incorporates two generators connected by the main wing that has a total length of 50 m (collectively, between the two sections). Additionally, a 660 m mooring cable extends from the sea floor to the bottom of the buoyancy tank. This design aims to enhance the efficiency and stability of the turbine in harnessing ocean current energy.

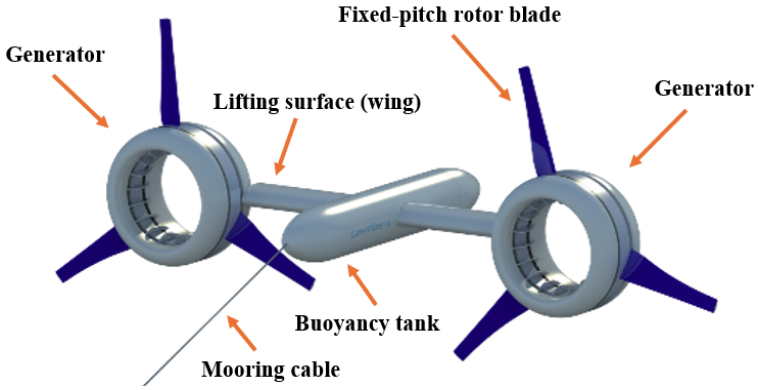

Fig 1. Schematic diagram of the ocean current turbine studied in this paper.

The dimensions and operational parameters of the designed OCT are summarized in Table I. It is configured for operation at approximately 75 m depth, securely moored to the seabed where the total water depth is 325 meters with both ballast tank sections 50% filled with water in a 1.6 m/s current. Table I details the moments of inertia about the center of gravity, total mass, and buoyancy characteristics of the OCT. Rotor blades are constructed using FX-83-W airfoils, with performance assessments based on a Reynolds number of 1×10^6. Blade specifications include twist angles ranging from 12.62° at the generator to 0.61° at the blade tip, with chord lengths varying from 1.37 m to 0.25 m. Additionally, the buoyancy tank adjusts the system's position in the water column, while electronics provide real-time monitoring and control. This tank holds 40 m^3 of ballast water, split evenly between forward and aft compartments, and is 15 m long with an external diameter of 2.2 m. The fore and aft ballast sections are each 6 m long, with the central 3 m section housing power conditioning electronics, computers, and ballast pumps. The total mass of the OCT is 224,160 kg, not counting ballast water, and the displaced mass is 264,800 kg, and the center of buoyancy is at set at the origin ([0, 0, 0] m), with the center of mass at [0, 0, 0.5] m. According to Table I, the total mass is calculated by the summation of two generators mass, main wing mass, two rotors mass, and two nacelles mass.

Table 1. Simulated Ocean Current Turbine Dimensions.

Dimensions	Unit	Value
Moment of inertia I_x	kgm^2	1.9044×10^7
Moment of inertia I_y	kgm^2	1.0714×10^6
Moment of inertia I_z	kgm^2	1.8927×10^7
Moment of Inertia of each rotor about x-axis I_x^r	kgm^2	3.5149×10^5
Total mass without ballast water	kg	224,160
Total displaced mass	kg	264.800
Total mass of buoyancy tank	kg	11,129
Buoyancy tank volume	m^3	40
Buoyancy tank length	m	15
Fore and aft ballast sections length of buoyancy tank	m	6
Electronics section length of buoyancy tank	m	3
Buoyancy tank external diameter	m	2.2
Thickness of buoyancy tank cylinder walls	cm	2
CG - CB in [x, y, z]	m	$[00, 0, 0.5]$
Rotor diameter Dr	m	20
Outer diameter of each generator	m	6
Inner diameter of each generator	m	4
Front to back length of each generator	m	4
Seawater displaced by each generator	m^3	44
Mass of each generator	kg	49610
Center of buoyancy of the generators	m	$[+0.5, +-13.1, 0]$
Total main wing span (each wing)	m	25
Non-rotating main wing average chord	m	5
Cable length	m	650
Cable mass per meter	kg/m	46
Cable diameter Dc	m	0.16
Rated power for each rotor	kW	600

2.2. Coordinate systems

To numerically simulate the Ocean Current Turbine (OCT), several coordinate systems are employed: an inertial coordinate system ($\bar{O}$), a body-fixed coordinate system ($\bar{B}$), momentum mesh coordinate systems ($\bar{M}$), shaft systems ($\bar{S}$), and rotor blade systems ($\bar{R}$), extensively detailed in [6]. The inertial coordinate system ($\bar{O}$) is positioned at mean ocean level, with its x-axis pointing north, y-axis eastward, and z-axis downward following the right-hand rule. The body-fixed coordinate system ($\bar{B}$) is located at the OCT's center of gravity, with its x-axis from tail to nose, z-axis downward relative to the turbine, and y-axis determined by the right-hand rule. coordinate systems ($\bar{O}$) and ($\bar{B}$) define the states of the OCT in the simulations. The remaining coordinate systems serve specific purposes: ($\bar{M}$) are centered at each rotor's axis of rotation, aligned with the x-axis axially, tangentially toward rotor rotation, and radially outward. These are crucial for the dynamic wake model, simulating velocity disturbances caused by rotor blades. Systems ($\bar{S}$), also at each rotor's center of rotation, rotate with the rotor. Their x_s-axes align with the x-axis, z_s-axes are perpendicular to rotor shafts and parallel to designated blades, and y-axes determined by the right-hand rule. Systems ($\bar{R}$) are located at each rotor blade section's quarter cord line, essential for calculating hydrodynamic forces. They relate to ($\bar{B}$) through ($\bar{M}$) and ($\bar{S}$), as detailed in [6].

Vectors are transformed from the inertial coordinate system ($\bar{O}$) to the body-fixed coordinate system ($\bar{B}$) by multiplying the inertial vector by the transformation matrix LOB, which is defined using the Euler angles as follows:

$$L_{\overline{OB}} = \begin{bmatrix} c_\alpha c_\theta & s_\alpha c_\theta & -s_\theta \\ c_\alpha s_\theta s_\varphi - s_\alpha c_\varphi & c_\alpha c_\varphi + s_\alpha s_\theta s_\varphi & c_\theta s_\varphi \\ c_\alpha s_\theta c_\varphi - s_\alpha s_\varphi & -c_\alpha s_\varphi + s_\alpha s_\theta c_\varphi & c_\theta s_\varphi \end{bmatrix}$$

where $\varphi, \theta \; and \; \alpha$ are roll angle, pitch angle and yaw angle, respectively. Also, $s_\varphi = \sin(\varphi)$ and $c_\varphi = \cos(\varphi)$, and the transformation matrix from the body-fixed coordinate system ($\bar{B}$) to the inertial coordinate system ($\bar{O}$) is $L_{\overline{BO}} = L^T_{L_{\overline{BO}}}$.

2.3. Equations of Motion

The motion of the numerically simulated OCT is described using 8-DOF. The equations of motion for the 6-DOF movement of the main body (excluding the rotors) of the OCT system were derived from [7]. These 6-DOF accelerations include the OCT's linear accelerations $\dot{u}$, $\dot{v}$, and $\dot{w}$, and angular accelerations $\dot{\omega}_x$, $\dot{\omega}_y$, and $\dot{\omega}_z$.

$$\begin{bmatrix} \dot{u} \\ \dot{v} \\ \dot{w} \end{bmatrix} = m^{-1} F \begin{bmatrix} i_{\bar{B}} \\ j_{\bar{B}} \\ k_{\bar{B}} \end{bmatrix} + \begin{bmatrix} u \\ v \\ \omega \end{bmatrix} \times \begin{bmatrix} \omega_x \\ \omega_y \\ \omega_z \end{bmatrix}$$

$$\begin{bmatrix} \dot{\omega}_x \\ \dot{\omega}_y \\ \dot{\omega}_z \end{bmatrix} = \begin{bmatrix} I_x^{-1} & 0 & 0 \\ 0 & I_y^{-1} & 0 \\ 0 & 0 & I_z^{-1} \end{bmatrix} (M \begin{bmatrix} i_{\bar{B}} \\ j_{\bar{B}} \\ k_{\bar{B}} \end{bmatrix} - \begin{bmatrix} (I_z - I_y)\omega_y . \omega_z \\ (I_x - I_z)\omega_z . \omega_x \\ (I_y - I_x)\omega_x . \omega_y \end{bmatrix})$$

where F denotes the vector of the total force in ($\bar{B}$), M is the vector of applied moments at the center of gravity of the OCT in ($\bar{B}$), and m is the total mass of the OCT. These forces and moments account for the total external forces and moments on the OCT, with the exception of the moment about the x-axis where the electromechanical torques on the OCT from each generator, τ_x^e replaces the hydrodynamic torque on each rotor, τ_x^h. ω_x, ω_y , and ω_z are the rotational velocities about the x, y, and z axes. The total force vector acting on the is the sum of gyroscopic force F_G, gravitational and buoyancy force F_{gb}, four wing forces F_ω, two rotor forces F_r , two nacelle forces F_n, and cable force F_c as follows:

$$F = F_G + F_{gb} + \sum_{m=1}^{4} F_{\omega,m} + \sum_{m=1}^{2} F_{r,m} + \sum_{m=1}^{2} F_{n,m} + F_c$$

The final 2-DOF of this OCT is the rotation of each rotor about the x-axis. The rotational acceleration of each rotor $\dot{\omega}_x^r$ is calculated as follows:

$$\dot{\omega}_x^r = \frac{\tau_x^r + \tau_x^s - qr(I_z^r - I_y^r)}{I_x^r}$$

where τ_x^s is the shaft moment about the x-axis induced by the generator on the rotor shaft, and I_y^r denotes the moment of inertia of each rotor about the y-axis. Finally, the overall degrees of freedom (DOFs) for the modeled system include three translational DOFs for each cable node in the cable model.

2.4. Gyroscopic Forcing

The gyroscopic force F_G caused by the rotational speed of each rotor around the x-axis, ω_x^r, is determined using:

$$F_G = I_x^r \begin{bmatrix} \omega_x^r \\ 0 \\ 0 \end{bmatrix} \times \begin{bmatrix} \omega_x \\ \omega_y \\ \omega_z \end{bmatrix}$$

2.5. Gravitational and buoyancy force:

This force F_{gb} is modeled using the transformation matrix from $\bar{B}$ to $\bar{O}$ (i.e., $L_{\overline{BO}}$), which can be expressed as:

$$F_{gb} = F_g + F_b = L_{\overline{BO}} \begin{bmatrix} 0 \\ 0 \\ mg \end{bmatrix} + L_{\overline{BO}} \begin{bmatrix} 0 \\ 0 \\ -B \end{bmatrix}$$

where m is the total mass of the OCT, g is the earth gravitational acceleration, and B is the variable total buoyancy force.

2.6. Hydrodynamic forcing

The hydrodynamic forces acting on the OCT, excluding the cable, are calculated for three types of components. These are defined as the wing forces (F_ω), which include forces on the main wing; the rotor forces (F_r), which encompass forces on the two rotors; and the nacelle forces (F_n), which pertain to the forces on the two nacelles.

Rotor Forces: In this numerical simulation, rotor forces are calculated using a Blade Element Momentum (BEM) rotor model that incorporates Dynamic Wake inflow calculations. This model determines the angle of attack for each rotor blade element and rotor mesh element (the mesh elements used to calculate rotor-induced flow perturbations). The angle of attack, denoted as α^{ij}, is computed from the equation $\alpha^{ij} = \varphi^{ij,ik} - \beta^{ij,ik}$, where $\beta^{ij,ik}$ represents the blade section pitch angle, and the relative flow angle $\varphi^{ij,ik}$ is given by $\varphi^{ij,ik} = tan^{-1}(-\frac{V_A^{ij}}{V_T^{ij}})$. Here, V_A and V_T are the axial and tangential components of the relative ocean velocity $V^{ij,ik}$. This relative ocean velocity is defined as the sum of three components: (i) the undisturbed ocean velocity, (ii) the blade motion-induced relative ocean velocity, and (iii) the wake-induced ocean velocity. Therefore, the forces on each of the two rotors, F_r, can be written as

$$F_{r,m} = \frac{1}{2}\rho \sum_{j=0}^{N_b}\sum_{i=0}^{N} L_{\overline{SB}}\, L_{\overline{RS}}^{ij} \begin{bmatrix} \delta r^i c^i C_T^{ij}\left(\left(V_A^{ij}\right)^2 + \left(V_T^{ij}\right)^2\right) \\ \delta r^i c^i C_T^{ij}\left(\left(V_A^{ij}\right)^2 + \left(V_T^{ij}\right)^2\right) \end{bmatrix}$$

where the index m refers to each of the two rotors, δ_r is the radial length, c is the cord length at the center of the section. Additionally, $L_{\overline{SB}}$ is a transformation matrix from shaft coordinate system to body-fixed coordinate system, and $L_{\overline{RS}}$ is also a transformation matrix from rotor blade coordinate system to body-fixed coordinate system

Wing Forces: The main wing is divided into N_ω discrete sections. Therefore, the force on each wing, F_ω, in the tangential, cross, and axial directions relative to the airfoils can be written as:

$$F_{\omega,m} = -\frac{1}{2}\rho A_{\omega,m} \begin{bmatrix} \sum_{i=1}^{N_{\omega,m}} C_t^i(\alpha)\left(V_m^i\right)^2 \\ 0 \\ \sum_{i=1}^{N_{\omega,m}} C_a^i(\alpha)\left(V_m^i\right)^2 \end{bmatrix}$$

where the index m refers to each of the four wings, V^i denotes the relative water speed with respect to a wing section calculated using only the normal and tangential components of relative water velocity, ρ = 1030 kg/m^3 is the water density, $C_t^i(\alpha)$ is the tangential drag coefficient of a wing section, $C_a^i(\alpha)$ is the axial drag coefficient, where both $C_t^i(\alpha)$ and $C_a^i(\alpha)$ are functions of angle of attack α. The $C_t^i(\alpha)$ and $C_a^i(\alpha)$ values are calculated using lift and drag coefficients for the utilized NACA 65-618 airfoil at a Reynolds number of 3 × 10^6 using X-Foil according to $C_t^i(\alpha)$= $C_D^i(\alpha)\cos(\alpha) - C_L^i(\alpha)\sin(\alpha)$ and $C_a^i(\alpha) = C_D^i(\alpha)\sin(\alpha) - C_L^i(\alpha)\cos(\alpha)$. The wing forces are then converted to forces in the body fixed frame using the pitch angle of each wing with respect to the body fixed coordinate system.

3. Results

In this section, the response of the Ocean Current Turbine (OCT) is presented for a depth independent flow field made up of a 1.6 m/s mean flow speed and a turbulence intensity of 15%. For all five simulations the OCT is started near an equilibrium depth of 75 m (variations due to turbulence) and each of the two-ballast tank sections, which hold up to 20 m^3 of water, are half filled with water (front = 10 m^3, back = 10 m^3) for the first 60-seconds of the numerical

simulation. After this, instantaneous ballast tank fill level changes are simulated to evaluate system response for the following 5 fill conditions: 1) **Baseline** case were water fill levels remain unchanged (front = 10 m^3, back = 10 m^3), 2) **Light** case were both tanks do not contain seawater (front = 0 m^3, back = 0 m^3), 3) **Max Negative Hydrostatic Moment** case where the front ballast section is filled with water and the back filled with air (front = 20 m^3, back = 0 m^3), 4) **Max Positive Hydrostatic Moment** case were the front tank is filled with air and the back with water, and 5) **Heavy** case were both tanks are filled with water (front = 20 m^3, back = 20 m^3). It is interesting to note that because of the placement the ballast tanks, center of gravity, and center of buoyancy cases 1, 2, and 5 all keep the center of buoyancy directly above the center of gravity. It is also interesting to note that the total mass of the system, including ballast water, is the same for cases 1, 3, and 4.

For the "Baseline" case (case 1), the elevation of the turbine fluctuates near a depth of 75 m with these variations primarily driven by turbulence. For the "Light" case (case 2) the turbine rises in elevation, with a final operating depth 65 m, 15 m above the final "Baseline" operating depth. For the "Heavy" case (case 5) the turbine elevation decreases, with a final operating depth 10 m below the "Baseline" case. For these three cases (Light, Baseline, and Heavy) produced power fluctuates around 680 kW and the OCT pitch angle fluctuates around -2.6°.

For cases where the total ballast water remains the same, but the amount each tank varies (Max Positive/Negative Hydrostatic Moment) the pitch angle of the OCT increases by 3.4° for the "Max Positive Hydrostatic Moment" case (case 4) and decreases by 1.7° for the "Max Negative Hydrostatic Moment" case (case 3) compared to the Baseline. The resulting final depth shows that the Negative Hydrostatic Moment case results in a 13-meter downward displacement in 7-minutes and that the Positive Hydrostatic Moment case results in a 2-meter upward displacement in 7-minutes, both referenced to Baseline. Like the other 3 cases, power production fluctuates around 680 kW.

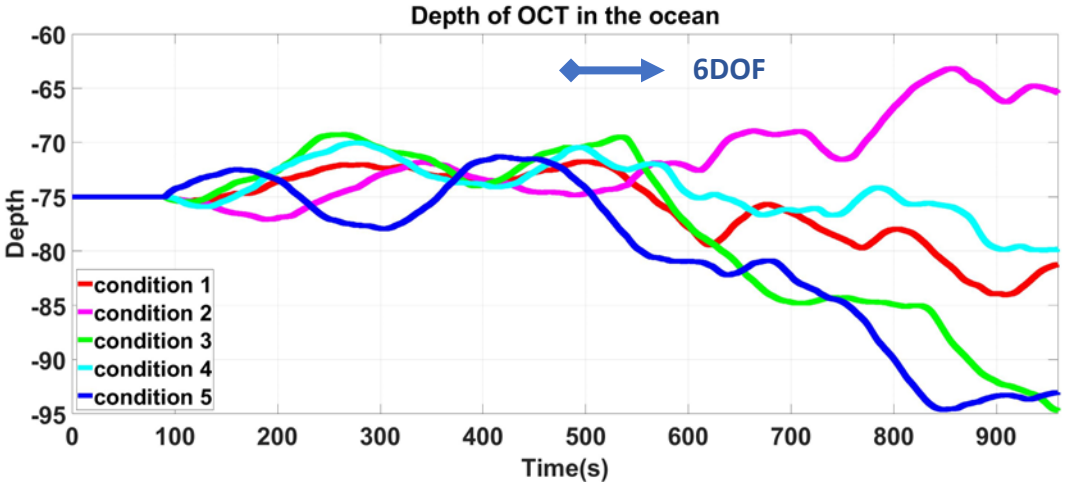

Fig 2. OCT (negative) depth [m] for 8-minute simulations where ballast tank fill levels are altered after the first 1-minute. *Times reference the 6DOF simulation run time which starts at Time 480 s.

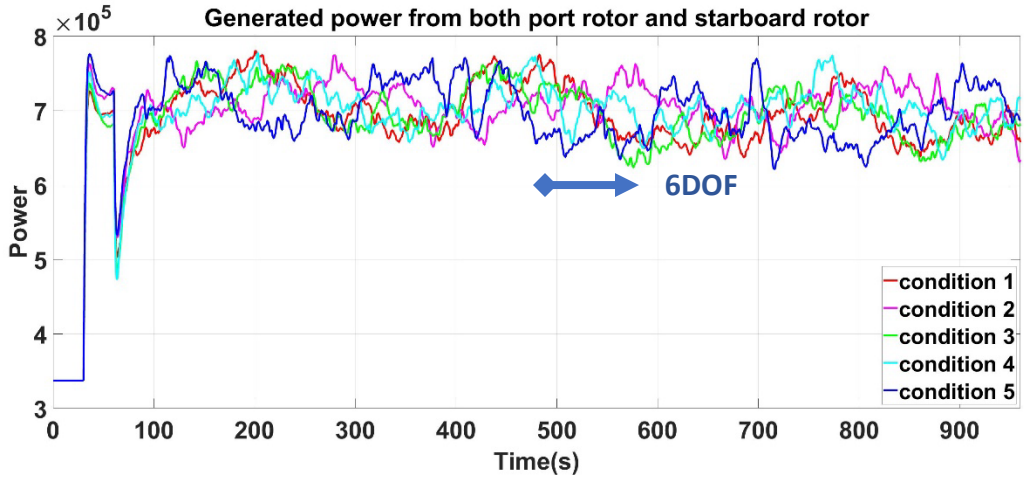

Fig 3. OCT power production [W] for 8-minute simulations where ballast fill levels are altered after the first 1-minute. *Times reference the 6DOF simulation run time which starts at Time 480 s.

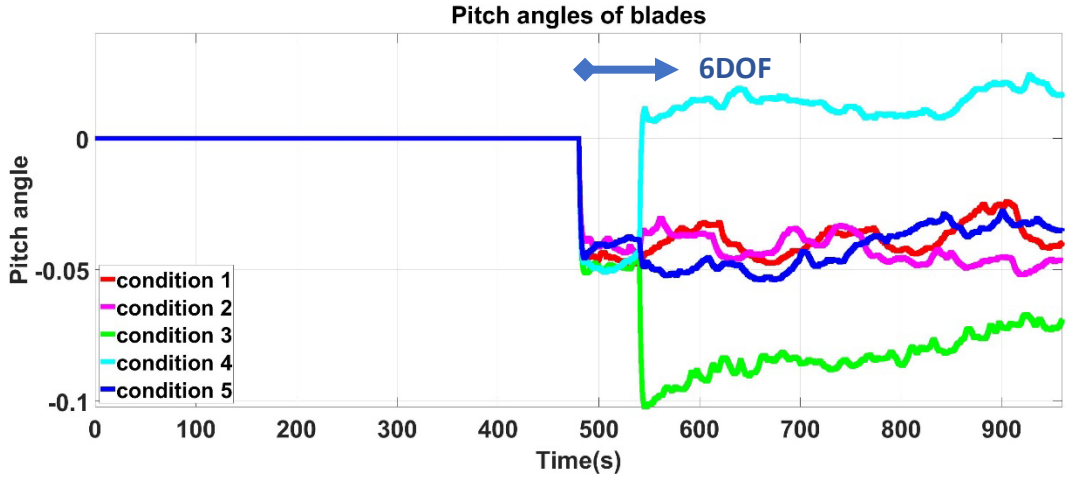

Fig 4. OCT pitch angle for 8-minute simulations where ballast tank fill levels are altered after the first 1-minute. *Times reference the 6DOF simulation run time which starts at Time 480 s.

4. Conclusion

In this work, we presented a dynamic model for a combined buoyancy and lifting surface-controlled ocean current turbine. Basic simulation results are provided to demonstrate the relationship between ballast tank fill levels and OCT response in a turbulent environment, demonstrating the simulation's utility for system evaluation which is important for OCT optimization and evaluation. Future work will focus on utilizing the developed numerical simulation for OCT optimization, analysis, and controler development.

5. Acknowledgements

This work was supported in part by the National Science Foundation under Grant No. CMMI-2145571 and the U.S. Department of Energy (DOE) under Grant No. CPS-40372.

6. References

[1] A. LiVecchi, A. Copping, D. Jenne, A. Gorton, R. Preus, G. Gill, R. Robichaud, R. Green, S. Geerlofs, S. Gore et al., "Powering the blue economy; exploring opportunities for marine renewable energy in maritime markets," US Department of Energy, Office of Energy Efficiency and Renewable Energy. Washington, DC, 2019.

[2] Y. Tang, J. VanZwieten, B. Dunlap, D. Wilson, C. Sultan, and N. Xiros, "In-stream hydrokinetic turbine fault detection and fault tolerant control - a benchmark model," in 2019 American Control Conference (ACC), 2019, pp. 4442–4447.

[3] X. Yang, K. A. Haas, and H. M. Fritz, "Theoretical assessment of ocean current energy potential for the gulf stream system," Marine Technology Society Journal, vol. 47, no. 4, pp. 101–112, 2013.

[4] X. Yang, K. Haas, and H. Fritz, "Evaluating the potential for energy extraction from turbines in the gulf stream system," Renewable energy, vol. 72, pp. 12–21, 2014.

[5] Y. Tang, Y. Zhang, A. Hasankhani, and J. VanZwieten, "Adaptive super-twisting sliding mode control for ocean current turbine-driven permanent magnet synchronous generator," in 2020 American Control Conference (ACC), 2020, pp. 211–217.

[6] J. VanZwieten, F. Driscoll, A. Leonessa, and G. Deane, "Design of a prototype ocean current turbine—part ii: flight control system," Ocean engineering, vol. 33, no. 11-12, pp. 1522–1551, 2006.

[7] J. H. VanZwieten, N. Vanrietvelde, and B. L. Hacker, "Numerical Simulation of an Experimental Ocean Current Turbine," IEEE Journal of Oceanic Engineering, vol. 38, no. 1, pp. 131–143, Jan. 2013.

[8] Hasankhani, Arezoo, et al. "Modeling and numerical simulation of a buoyancy controlled ocean current turbine." *International Marine Energy Journal* 4.2 (2021).